Vol 18 No 6, June 2009
1674-1056/2009/18(06)/2258-06

Chinese Physics B

© 2009 Chin. Phys. Soc.
and IOP Publishing Ltd

Size dependence of biexciton binding energy in single InAs/GaAs quantum dots*

Dou Xiu-Ming(窦秀明)[a], Sun Bao-Quan(孙宝权)[a]†,
Huang She-Song(黄社松)[a], Ni Hai-Qiao(倪海桥)[a],
Niu Zhi-Chuan(牛智川)[a], Yang Fu-Hua(杨富华)[a], and Jia Rui(贾 锐)[b]

[a] *SKLSM, Institute of Semiconductors, Chinese Academy of Sciences, Beijing* 100083, *China*
[b] *Laboratory of Nano-Fabrication and Novel Devices Integrated Technology, Institute of Microelectronics, Chinese Academy of Sciences, Beijing* 100029, *China*

(Received 27 June 2008; revised manuscript received 27 November 2008)

This paper studies the size dependence of biexciton binding energy in single quantum dots (QDs) by using atomic force microscopy and micro-photoluminescence measurements. It finds that the biexciton binding energies in the QDs show "binding" and "antibinding" properties which correspond to the large and small sizes of QDs, respectively. The experimental results can be well interpreted by the biexciton potential curve, calculated from the exciton molecular model and the Heitler–London method.

Keywords: biexcition binding energy, single quantum dots, exciton molecular model, Heitler–London method
PACC: 3520V, 7280E, 7320D

1. Introduction

Self-assembled semiconductor quantum dots (QDs) have been intensively studied in the past few years.[1−3] Atomic-like features and narrow lines of the luminescence have been observed in the exciton emission spectra due to the full spatial three-dimensional confinement.[4−11] Based on these unique features, QDs have promising potential in many applications, such as low-threshold laser,[12,13] optical amplifier,[14] and solid-state single photon source.[15−19]

In this paper, we have studied the size dependence of the biexciton binding energy in single quantum dots by using atomic force microscopy (AFM) and photoluminescence (PL). Exciton and biexciton emissions are identified by the excitation power-dependent PL spectra. The biexciton binding energies in the QDs, denoted as E_{2X}, show "binding" and "antibinding" properties, corresponding to the large QDs (LQDs) and the small QDs (SQDs), respectively. Based on the exciton molecular model and the Heitler–London method, we calculate E_{2X}, as a function of the separate distance between the two excitons.

2. Experimental details

Two self-assembled InAs QD samples A and B were grown by molecular beam epitaxy on semi-insulating GaAs substrates. Samples A (B) consist of, in sequence, 500 nm GaAs buffer layer, 2.35 (2.25) monolayer (ML) of InAs, 300 nm GaAs layer, and top QD layer formed by the same growth conditions as the first QD layer for AFM measurements. Details of the growth process can be found elsewhere.[20] In Fig.1(a), AFM image shows that the LQDs in sample A have a uniformly sized distribution, and five LQDs (marked by 1, 2, 3, 4, 5) with the base length of about 60 nm and the heights of 9.5, 9.8, 7.6, 7.5, and 8.3 nm, respectively, are selected for calculating the E_{2X}. Whereas sample B has both large and small QDs, indicated in Fig.1(b). Also, five SQDs (marked by 6, 7, 8, 9, and 10) with the base length of about 40 nm and heights of 2.6, 1.8, 1.3, 1.0, and 0.8 nm, respectively, are used to calculate the E_{2X}.

Ensemble QD PL spectra were measured by a Fourier spectrometer. The samples, mounted in a closed cycle cryostat down to 10 K, were excited by an He–Ne laser and the PL signals were collected by an

*Project supported by the National Natural Science Foundations of China (Grant Nos O69C041001 and 2007CB924904).
†Corresponding author. E-mail: bqsun@semi.ac.cn

LN-cooled Ge detector. Single QD micro-PL spectra were measured by a low-temperature scanning confocal microscopy. Samples were placed in a continuous flow liquid helium cryostat cooled to 5 K. A microscope objective (NA: 0.5) was used to focus He–Ne laser on the QDs and collect the PL. The luminescence was dispersed by a 0.5 m monochromator and detected by an Si-CCD. The spatial resolution of the micro-PL setup is about 1 μm.

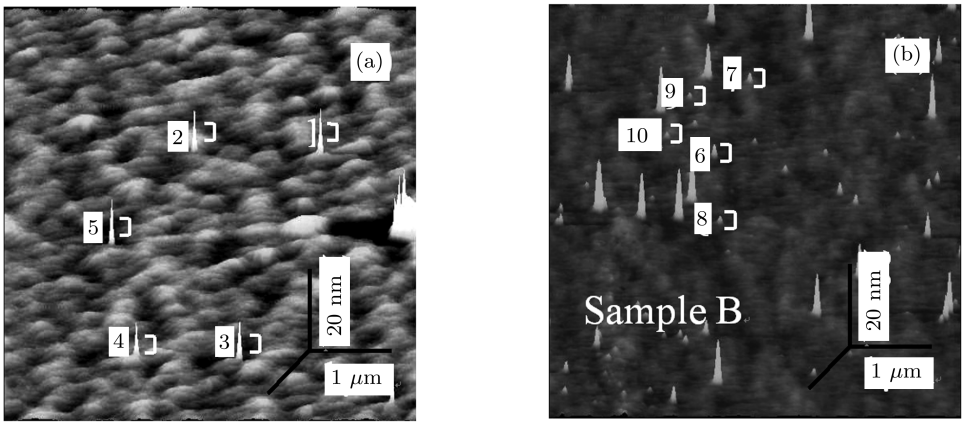


Fig.1. 5×5 μm^2 AFM images of the samples A (a) and B (b), where the selected QDs are marked by brackets and numbers.

3. Results and discussion

Figure 2(a) displays the PL spectra of the sample A measured at 10 K. The ground-state exciton transition energy (GSETE) is 1.005 eV with a full width at half maximum (FWHM) of 22 meV, indicating that the sizes of the QDs have a uniform distribution. This description is consistent with the AFM results. In order to shift the GSETE of the QDs to the response range of the Si-CCD, the QDs were exposed to a 30 s rapid thermal annealing at 950 °C. The annealing-induced intermixing between the InAs QDs and the GaAs barrier, shifts the GSETE to the higher energy of 1.329 eV.[21] The PL signals marked by a, b, c are the emissions from three large QDs (LQDa, LQDb, LQDc), whose micro-PL spectra are shown in Fig.3(b). Figure 2(b) shows the PL spectrum of the sample B measured at 10 K. A broad and weak exciton emission band at lower energy regime is found, which means a broad distribution of the QD sizes, as observed in the AFM image. Also, the PL signals marked by d, e, and f are the emissions from three small QDs (SQDd, SQDe, SQDf), whose micro-PL spectra are shown in Fig.4(b). In addition, a very strong emission peak on the higher energy side originates from the wetting layer.

Excitation power dependence of the micro-PL for LQDa is presented in the inset of Fig.3(a). At low excitation power of 9.4 nW, the peak X with an emission energy of 1.366 eV is observed. As the excitation power increases to 40 nW, a new emission peak 2X appears at an energy of 4.4 meV lower than the peak X. To identify the emissions of the peaks X and 2X, the integrated PL intensities, I, as a function of the excitation power P, are plotted in Fig.3(a). At low excitation power limit, I can be fitted by a relation of $I \propto P^n$, with n about 0.84 and 1.62 for peaks X and 2X, respectively. Compared with the emission of the peak X, we find that peak 2X occurs and saturates at higher excitation power, and both have a relation of $I_{2X} \propto I_X^2$. Thus, the peaks X and 2X are assigned to the emissions of the exciton and biexciton, respectively. The deviation from the ideal linear and quadratic excitation power dependence of the exciton and biexciton emissions has also been observed in QD emitting at 1300 nm.[22] The LQDb and LQDc also demonstrate the similar micro-PL spectra, as indicated in Fig.3(b), where the exciton emission energies are 1.366, 1.364 and 1.345 eV for LQDa, b and c, respectively. Compared with excitons, all biexcitons

have lower emission energies and correspond to the binding energies of about –4.4, –3.8, and –4.5 meV for LQDa, b, and c, respectively. In this case the biexciton state is called "binding" state. For clearly showing the values of E_{2X}, the exciton PL peaks in Fig.3(b) are shifted to the zero position. The other emission peaks marked X* in Fig.3(b) may be related to the charged exciton emission.[23]

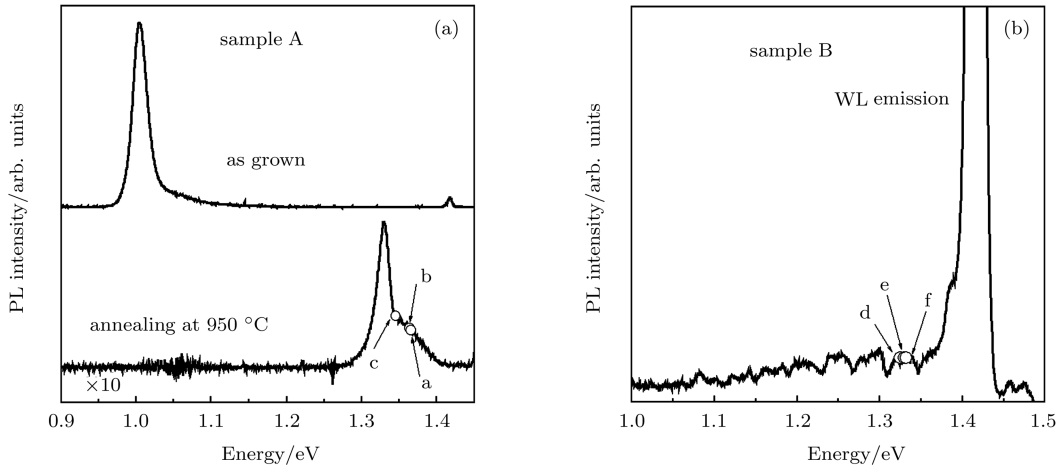


Fig.2. The PL spectra of the ensemble QDs measured at 10 K for as grown and annealed samples A (a) and sample B (b) with the excitation power of about 1 μW. The arrows mark the PL signals of the QDs observed in micro-PL measurements.

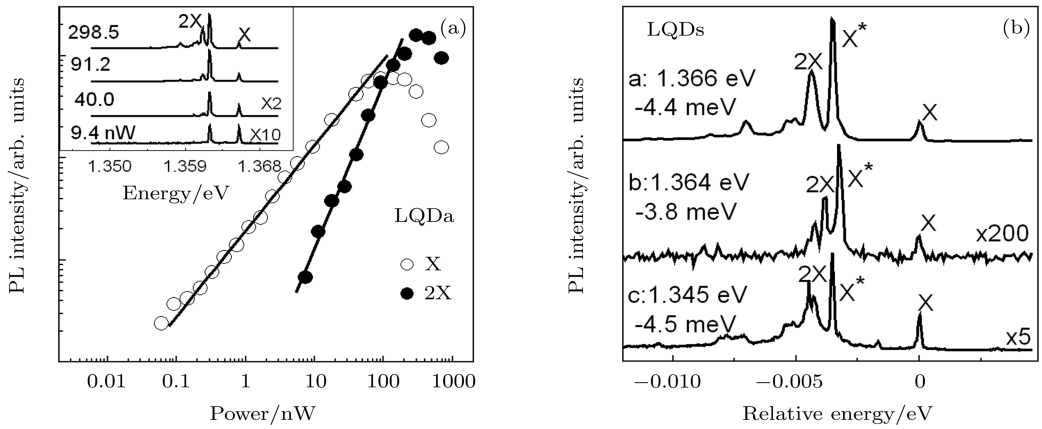


Fig.3. (a) Log-log plots of the integrated PL intensity of LQDa as a function of the excitation power. Inset: excitation power-dependent micro-PL spectra measured at 5 K. (b) PL spectra of three LQDs, shifted in energy to align the exciton emission peaks. The exciton emission energy and the biexciton binding energy are given for LQDa, b, and c.

In the inset of Fig.4(a), the excitation power-dependence of the micro-PL for SQDd is shown. At low excitation power of 5 nW, an emission peak X is observed at 1.325 eV. With the increase of the excitation power, the peak 2X appears, which is about 6 meV higher than the peak X. Similar to the case of Fig.3(a), the integrated PL intensity as a function of excitation power is plotted in Fig.4(a). Depending on the linear fitting results of the experimental data, $I \propto P^n$, we find that the exponential n is about 0.954 and 1.964 for peaks X and 2X, respectively. Then peaks X and 2X are attributed to the exciton and biexciton emissions, respectively. The micro-PL spectra of SQDd, e, and f with the exciton emission energies of 1.325, 1.330 and 1.332 eV, respectively, are shown in Fig.4(b). The PL spectra show that the biexcitons have positive binding energies, so called "antibinding" states, and correspond to the binding energies of about 5.9, 7.3, and 5.4 meV for SQDd, e, and f, respectively. Here all exciton emission PL peaks are shifted to the zero position.

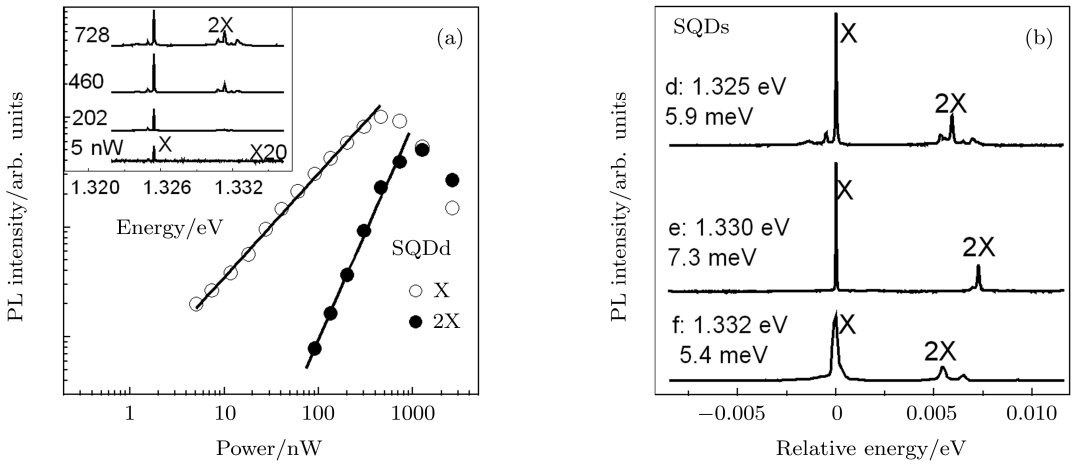


Fig.4. (a) Log-log plots of the integrated PL intensity of SQDd as a function of the excitation power. Inset: excitation power-dependent micro-PL spectra measured at 5 K. (b) PL spectra of three SQDs, shifted in energy to align the exciton emission peaks. The exciton emission energy and the biexciton binding energy are given for SQDd, e, and f.

As discussed above, there are "binding" and "antibinding" biexcitons in the QDs, which should be related to the sizes of the QDs. It is in fact that for sample A, the annealing-induced blueshift of the GSETE is most originating from the intermixing between the GaAs and InAs layers. In this process, InGaAs QDs are formed and the band-gap of the QDs is also increased. This leads to the decrease of the confinement potential but the geometric sizes of the QDs should not alter significantly. This description is confirmed by the PL spectra of the annealed ensemble QDs, i.e., the number of the confined states in QDs remains unchanged and the energy separation between the confined states decreases. Thus, in sample A, the LQDs remain the large geometric sizes after annealing. But, in sample B, the QDs have a broad sized distribution. The SQDs, having higher PL emission energies, are selected for micro-PL measurements.

Biexciton is a bound state of two excitons and the binding energy is defined as the energy gain due to the correlation and exchange interactions between electrons and holes. In order to investigate the influence of three-dimensional spatial confinement on the biexciton binding energy, we use an exciton molecular model to calculate E_{2X} as a function of separate distance between two excitons in bulk InAs. Then we get the E_{2X} in QDs by using exciton binding energy in QDs instead of bulk InAs. Finally, the calculated results are compared with the experimental data for testing the validity of the model.

The Hamiltonian of a biexciton system in bulk InAs containing two electrons and two holes[24−26] are given by

$$\begin{aligned} H &= -\frac{\hbar^2}{2m_{\mathrm{e}}^*}(\nabla_1^2+\nabla_2^2) - \frac{\hbar^2}{2m_{\mathrm{h}}^*}(\nabla_a^2+\nabla_b^2) \\ &\quad + \frac{e^2}{\varepsilon}\left(\frac{1}{r_{12}} + \frac{1}{r_{ab}} - \frac{1}{r_{1a}} - \frac{1}{r_{1b}} - \frac{1}{r_{2b}} - \frac{1}{r_{2a}}\right), \end{aligned} \quad (1)$$

where indexes 1, 2 stand for the two electrons, and a, b for the two holes, r_{12}, r_{ab}, r_{1a}, r_{1b}, r_{2b}, r_{2a} for the corresponding distances between all four particles, and ε is permittivity. For bulk InAs, the effective mass of the hole is about 10 times larger than the electron one, i.e. $m_{\mathrm{h}}^* \sim 10\ m_{\mathrm{e}}^*$. It is reasonable to treat the exciton as a hydrogen atom and the biexciton as a hydrogen molecule, and adopt the Heitler–London method to deal with the Coulomb interaction between the electrons and holes. So, the Hamiltonian of a biexciton system can be reduced to

$$\begin{aligned} H &= \left(-\frac{\hbar^2}{2m_{\mathrm{e}}^*}\nabla_1^2 - \frac{e^2}{\varepsilon r_{1a}}\right) + \left(-\frac{\hbar^2}{2m_{\mathrm{e}}^*}\nabla_2^2 - \frac{e^2}{\varepsilon r_{2b}}\right) \\ &\quad + \frac{e^2}{\varepsilon}\left(\frac{1}{r_{12}} + \frac{1}{r_{ab}} - \frac{1}{r_{1b}} - \frac{1}{r_{2a}}\right), \end{aligned} \quad (2)$$

where the first and second terms represent the Hamiltonians of the electron 1 in the potential of the hole a and the electron 2 in the potential of the hole b, respectively. These two terms describe two isolated excitons, and mean that there is no interaction between them.

The exciton binding energy is denoted by E_0 and the exciton wavefunction is $\varphi(r) = \frac{1}{\sqrt{\pi a_0^3}} e^{-r/a_0}$, where a_0 is the exciton Bohr radius. The third term represents the Coulomb interaction energy between the electrons and the holes. Taking the electron spin into account, we find that two electrons can form singlet and triplet states. The singlet state of the biexciton forms the ground state and the corresponding wavefunction $\Psi_{ab}(1,2)$ is given by

$$\begin{aligned}\Psi_{ab}(1,2) &= C[\varphi_a(1)\varphi_b(2) + \varphi_b(1)\varphi_a(2)] \\ &\quad \times[\chi_\uparrow(1)\chi_\downarrow(2) - \chi_\downarrow(1)\chi_\uparrow(2)], \end{aligned} \quad (3)$$

where inside the first bracket is the symmetric spatial wavefunction of two electrons and inside the second bracket is the asymmetric spin wavefunction of two electrons. Using this wavefunction, we can calculate the E_{2X} in the biexciton system. Therefore, the total energy of the biexciton is given by

$$\begin{aligned} E &= 2E_0 + E_{2X} \\ &= 2E_0 + \frac{Q+J}{1+S}, \end{aligned} \quad (4)$$

where S is an overlap integral, Q a Coulomb integral, and J an exchange integral. They can be expressed as

$$\begin{aligned} S &= \int \varphi_a(1)\varphi_b(2)\varphi_a(2)\varphi_b(1)\mathrm{d}\tau_1\mathrm{d}\tau_2 = e^{-2\zeta}\left(1+\zeta+\frac{1}{3}\zeta^2\right)^2, \\ Q &= \frac{e^2}{\varepsilon r_{ab}} + \int \frac{e^2}{\varepsilon r_{12}}\varphi_a^2(1)\varphi_b^2(2)\mathrm{d}\tau_1\mathrm{d}\tau_2 - 2\int \frac{e^2}{\varepsilon r_{a2}}\varphi_b^2(2)\mathrm{d}\tau_2 \\ &= 2E_0 e^{-2\zeta}\left(\frac{5}{8} + \frac{1}{\zeta} - \frac{3}{4}\zeta - \frac{1}{6}\zeta^2\right), \\ J &= \frac{e^2}{\varepsilon r_{ab}}S + \int \frac{e^2}{\varepsilon r_{12}}\varphi_a(1)\varphi_b(2)\varphi_a(2)\varphi_b(1)\mathrm{d}\tau_1\mathrm{d}\tau_2 - 2\int \frac{e^2}{\varepsilon r_{a1}}\varphi_a(2)\varphi_b(2)\varphi_a(1)\varphi_b(1)\mathrm{d}\tau_1\mathrm{d}\tau_2 \\ &= 2E_0 e^{-2\zeta}\left[\frac{1}{\zeta}\left(1+\zeta+\frac{1}{3}\zeta^2\right)^2 - 2(1+\zeta)\left(1+\zeta+\frac{1}{3}\zeta^2\right) + \frac{5}{8}\left(1+\zeta+\frac{1}{3}\zeta^2\right)\right], \end{aligned} \quad (5)$$

where $\zeta = \frac{r_{ab}}{a_{ex}}$.

Based on the expressions of Eqs.(4) and (5), Figure 5 plots the binding energy curve of the biexciton as a function of the separate distance between two excitons, where the unit of the X-axis is the exciton Bohr radius a_0, about 25 nm, and the unit of the Y-axis is the exciton binding energy in InAs QDs E_0, about 10 meV,[27] instead of that in InAs bulk for considering the influence of three-dimensional spatial confinement. The biexciton binding energy curve shows that the exciton-exciton interaction is attractive and a "binding" biexciton is formed when $r_{ab} > 0.8\ a_0$. Whereas it is repulsive between two excitons and forms a so-called "antibinding" biexciton when $r_{ab} < 0.8\ a_0$. In order to understand the relation between the geometric sizes of the QDs and the states of biexcitons, it is reasonable to define the effective diameter of the QDs, $D = (d^2 \cdot h)^{1/3}$, where d and h are the base length and the height of the QDs, respectively. Following this expression and the sizes of the QDs given by AFM, we calculate the Ds, which are $1.30a_0$, $1.31a_0$, $1.21a_0$, $1.20a_0$, and $1.24a_0$ for LQD1, 2, 3, 4, and 5, respectively, indicated by open triangles in Fig.4. For SQDs, the calculated Ds are $0.64a_0$, $0.57a_0$, $0.51a_0$, $0.47a_0$,

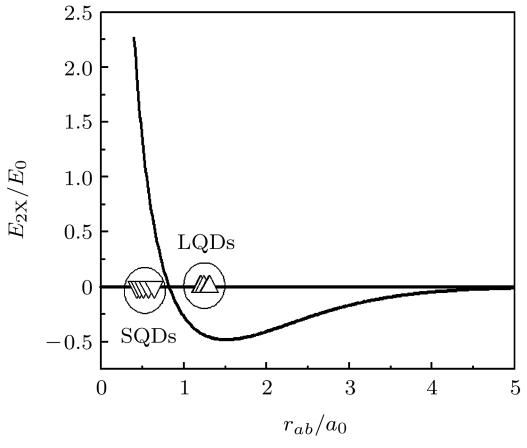


Fig.5. Calculated biexciton binding energy curve as a function of the separate distance between the two excitons. The open triangles represent the effective diameters of LQDs selected in Fig.1(a), and the reverse open triangles represent the effective diameters of SQDs selected in Fig.1(b).

and $0.43a_0$ for SQD6, 7, 8, 9, and 10, respectively, indicated by reverse open triangles in Fig.4. Then the corresponding average Ds are $1.20a_0$ and $0.52a_0$ for LQDs and SQDs, respectively. From the biexciton binding energy curve, it is found that the average biexciton binding energies for LQDs and SQDs are about –4.4 meV ($-0.44E_0$) and 11.8 meV ($1.18E_0$), respectively. The calculated results are close to the experimental values of E_{2X}, as indicated in Figs.3(b) and 4(b), this means that the proposed simple model is valid and can be used to study the biexciton binding energies of the QDs.

4. Conclusion

Based on the excitation power-dependence of the micro-PL, the excitons and the biexcitons are identified. The "binding" and "antibinding" biexcitons are observed corresponding to the LQDs and SQDs, respectively. Both the exciton molecular model and the Heitler–London method are employed to calculate the biexciton binding energy curve as a function of the separate distance between the two excitons. This curve can be used to interpret an attractive or a repulsive interaction between the excitons when biexciton is confined in QDs.

References

[1] Michler P (ed) 2003 *Single Quantum Dots* (Berlin: Springer-Verlag)

[2] Bimberg D, Grundmann M and Ledentsov N N 1999 *Quantum Dot Heterostructures* (Chichester: Wiley)

[3] Jacak L, Hawrylak P and Wójs A 1998 *Quantum Dots* (Berlin: Springer-Verlag)

[4] Marzin J Y, Gerard J M, Izraël A, Barrier D and Bastard G 1994 *Phys. Rev. Lett.* **73** 716

[5] Gammon D, Snow E S, Shanabrook B V, Katzer Q S and Park D 1996 *Phys. Rev. Lett.* **76** 3005

[6] Bayer M, Stern O, Hawrylak P, Fafard S and Forchel A 2000 *Nature* (London) **405** 923

[7] Dekel E, Gershoni D, Ehrenfreund E, Spektor D, Garcia J M and Petroff P M 1998 *Phys. Rev. Lett.* **80** 4991

[8] Landin L, Miller M S, Pistol M E, Pryor C E and Samuelson L 1998 *Science* **280** 262

[9] Finley J J, Ashmore A D, Lemaître A, Mowbray D J, Skolnick M S, Itskevich I E, Maksym P A, Hopkinson M and Krauss T F 2001 *Phys. Rev.* B **63** 073307

[10] Rodt S, Heitz R, Schliwa A, Sellin R L, Guffarth F and Bimberg D 2003 *Phys. Rev.* B **68** 035331

[11] Huang S S, Niu Z C, Zhan F, Ni H Q, Zhao H, Wu D H and Sun Z 2008 *Chin. Phys.* B **17** 323

[12] Peng H L, Han Q, Yang X H and Niu Z C 2007 *Acta Phys. Sin.* **56** 863 (in Chinese)

[13] Bimberg D and Ribbat C 2003 *Microelectronics J.* **34** 323

[14] Uskov A V, O'Reilly E P, Laemmlin M, Ledentsov N N and Bimberg D 2005 *Opt. Commun.* **248** 211

[15] Michler P, AKiraz, Becher C, Schoenfeld W V, Petroff P M, Zhang L D, Hu E and Imamoğlu A 2000 *Science* **290** 2282

[16] Santori C, Pelton M, Solomon G, Dale Y and Yamamoto Y 2001 *Phys. Rev. Lett.* **86** 1502

[17] Zwiller V, Blom H, Jonsson P, Panev N, Jeppesen S, Tsegaye T, Goobar E, Pistol M E, Samuelson L and Björk G 2001 *Appl. Phys. Lett.* **78** 2476

[18] Thompson R M, Stevenson R M, Shields A J, Farrer I, Lobo C J, Ritchie D A, Leadbeater M L and Pepper M 2001 *Phys. Rev.* B **64** R201302

[19] Mirin R P 2004 *Appl. Phys. Lett.* **84** 1260

[20] Huang S S, Niu Z C, Ni H Q, Xiong Y H, Zhan F, Fang Z D and Xia J B 2007 *J. Crystal Growth* **301** 751

[21] Fafard S and Allen C Nì 1999 *Appl. Phys. Lett.* **75** 2374

[22] Alloing B, Zinoni C, Zwiller V, Li L H, Monat C, Gobet M, Buchs G, Fiore A, Pelucchi E and Kapon E 2005 *Appl. Phys. Lett.* **86** 101908

[23] Lomascolo M, Vergine A, Johal T K, Rinaldi R, Passaseo A, Cingolani R, Patanè S, Labardi M, Allegrini M, Troiani F and Molinari E 2002 *Phys. Rev.* B **66** R041302

[24] Jin S S 1980 *Elements and Applications of Quantum Chemistry* (Shanghai: Shanghai Science and Technology Press), p151 (in Chinese)

[25] Li Z Z 1985 *Theory of Solid* (Beijing: Higher Education Press), p 358 (in Chinese)

[26] Haken H and Wolf H C 1995 *Molecular Physics and Elements of Quantum Chemistry* (Berlin: Springer-Verlag), p 51

[27] Grundmann M, Stier O and Bimberg D 1995 *Phys. Rev.* B **52** 11969